Dynamic Wavelength Conversion in Copropagating Slow-Light Pulses

K. Kondo and T. Baba
Department of Electrical and Computer Engineering, Yokohama National University, 79-5 Tokiwadai, Hodogayaku, Yokohama 240-8501, Japan
(Received 16 December 2013; published 6 June 2014)

Dynamic wavelength conversion (DWC) is obtained by controlling copropagating slow-light signal and control pulse trajectories. Our method is based on the understanding that conventional resonator-based DWC can be generalized, and is linked to cross-phase modulation. Dispersion-engineered Si photonic crystal waveguides produce such slow-light pulses. Free carriers generated by two-photon absorption of the control pulse dynamically shift the signal wavelength. Matching the group velocities of the two pulses enhances the shift, elongating the interaction length. We demonstrate an extremely large wavelength shift in DWC (4.9 nm blueshift) for the signal wavelength. Although DWC is similar to the Doppler effect, we highlight their essential differences.

DOI: 10.1103/PhysRevLett.112.223904 PACS numbers: 42.70.Qs, 42.25.Bs, 42.79.Nv, 42.82.-m

The wavelength of light is shifted when the index of the medium through which it travels (modal index) changes instantaneously. This is called dynamic wavelength conversion (DWC) and was first discussed theoretically [1,2] and then demonstrated experimentally by using plasma dispersion of free carriers [3,4] for light localized in resonators [Fig. 1(a)]. It was also observed for light propagating in waveguides [5–7], for which the mechanism responsible for DWC is identical to the resonator case because the waveguide index changes simultaneously and uniformly.

DWC has been understood as a process that differs from nonlinear processes, such as parametric four-wave mixing and Kerr-based cross-phase modulation (XPM) in fibers [8], because it (1) targets light localized in microdevices, as mentioned above, (2) achieves a 100% efficiency in the ideal case, maintaining spectral shape and coherency, (3) does not require large nonlinear effects, and (4) can be induced not only optically but also electrically [9] and mechanically [10]. Although attractive, a drawback of DWC is its small wavelength shift $\Delta\lambda$. Since $\Delta\lambda$ strongly depends on the index change Δn such that $\Delta\lambda/\lambda \approx \Delta n/n$ [2], it is no greater than 1 to 2 nm for $\lambda \approx 1.55$ μm.

To overcome this drawback, we propose a different type of DWC, which we refer to as trajectory-dependent DWC (TD-DWC). In TD-DWC, the optical signal pulse is not localized but propagates in a waveguide together with the temporal change in index, generating continuous DWC. In this approach, $\Delta\lambda$ depends not only on Δn but also on the trajectory of the pulse and index change. To generate the propagating index change, we use the plasma dispersion of free carriers induced by two-photon absorption (TPA) of a slow-light pulse (control pulse). We also produce another slow-light pulse at a different wavelength as the signal and arrange for these two pulses to copropagate, as shown in Fig. 1(b). For this purpose, we use low-dispersion slow-light pulses in a Si lattice-shifted photonic-crystal waveguide (LSPCW), wherein the third rows of air holes in the photonic-crystal slab are shifted longitudinally [11,12]. The incident control pulse is spatially compressed due to the slow-light effect, and its peak intensity is enhanced internally. This causes large TPA in Si at $\lambda \approx 1.55$ μm, generating free carriers and reducing the index [12,13]. If the signal pulse overlaps with the control pulse, its wavelength is blueshifted. If the overlap is maintained by matching group velocities, $\Delta\lambda$ is enhanced beyond the Δn limit, within the range of acceptable losses. Thus, TD-DWC allows the limit of the conventional DWC to be overcome.

We now discuss a theoretical expression of TD-DWC. The phase shift $\Delta\phi$ in the signal pulse is given by

$$\Delta\varphi = \int_C \Delta k(z,t)dz, \tag{1}$$

where $\Delta k(z,t)$ is the local change induced by the control pulse of the signal-pulse wave number at position z and

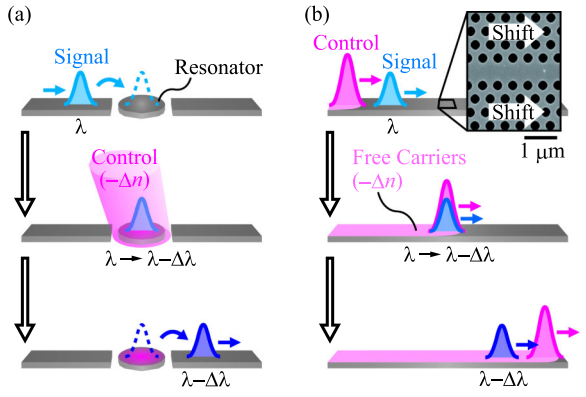

FIG. 1 (color online). Schematic of DWC by free-carrier generation. (a) Conventional DWC by resonator. (b) TD-DWC by copropagating pulses in LSPCW [inset to (b) shows scanning electron micrograph of fabricated LSPCW].

time t, and C is the trajectory of the signal pulse, which satisfies $t = (n_g/c)z$ for the group index $n_g = c(\partial k/\partial\omega)$, where c is the speed of light in vacuum. Subsequently,

$$\Delta\varphi = \int_C \frac{\omega}{cn} c \frac{\partial k}{\partial\omega}\frac{n}{\omega}\frac{\partial\omega}{\partial n}\Delta n(z,t)dz = \frac{\omega n_g \xi}{cn}\int_C \Delta n(z,t)dz, \quad (2)$$

where $\xi = (n/\omega)(\partial\omega/\partial n)$ is the dependence of the normalized photonic-band frequency on the normalized change in index. The normalized photonic-band frequency is determined by the waveguide structure and is almost constant over the narrow frequency range considered for TD-DWC. From Eq. (2), $\Delta\lambda$ is

$$\Delta\lambda = \lambda\frac{\Delta\omega}{\omega} = \frac{\lambda}{\omega}\frac{\partial\varphi}{\partial t} = \frac{\lambda n_g\xi}{cn}\int_C \frac{\partial}{\partial t}\Delta n(z,t)dz \quad (3)$$

$$= \frac{\lambda\xi}{n}\int_C \frac{\partial}{\partial t}\Delta n(z,t)dt. \quad (4)$$

The integral goes from $z = 0 - L(t = 0 - T)$, where the overlap of the two pulses begins, to L where it ends; i.e., the interaction length is L and the interaction time is T. The quantities L and T are determined by the input timing, group velocities, and/or waveguide length.

Applying Eq. (4) to light trapped in a resonator can be interesting. In this case, z is fixed by the resonator, so the integral and derivative cancel each other, leading to $\Delta\lambda/\lambda \approx \Delta n/n$ for conventional DWC. This means that conventional DWC is an extreme case of TD-DWC (in other words, TD-DWC is more general than conventional DWC). Figure 2 shows the spatiotemporal dynamics of Δn and its time derivative for both conventional DWC and TD-DWC. Red profiles depict the change in index, which is fixed for conventional DWC but moves for TD-DWC. Blue dashed lines and striped areas depict the trajectory of the signal pulse and its projection onto the change in index, respectively. When the blue line crosses the red profile at an oblique angle, TD-DWC increases the area (and thus $\Delta\lambda$).

On the basis of the discussion thus far, TD-DWC appears similar to XPM. In fact, this is accurate, which tells us that conventional DWC is actually linked to XPM. To clarify their similarities and differences, we now compare the definitions and features of XPM and DWC. XPM is an all-optical phenomenon in a medium, and Kerr-based XPM, which is the most common type of XPM, usually broadens the signal spectrum. XPM could be extended to XPM accompanied by plasma dispersion, such as when self-phase modulation with plasma dispersion adds spectral asymmetry and causes a blueshift [14] or when soliton pulses are produced, leading to a pure spectral blueshift without broadening [15]. DWC, however, may be generated by any Δn and is not limited to optical processes. Even TD-DWC may occur if a propagating Δn is generated by a traveling microwave, acoustic wave, and so on. In addition, we show below a pure spectral shift that occurs without a soliton, which is commonly thought to be a key feature of DWC. Therefore, TD-DWC is more appropriately categorized as DWC, even if it is similar to XPM.

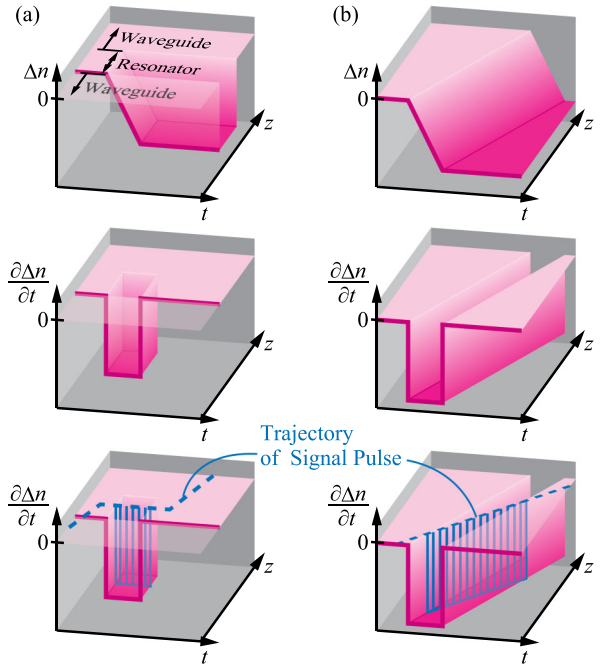

FIG. 2 (color online). Schematic of spatiotemporal change in index (top panels) and its derivation (middle and lower panels). This generates DWC according to Eqs. (3) and (4). (a) Conventional DWC and (b) TD-DWC. Blue dashed lines indicate the signal-pulse trajectory.

We begin by simulating TD-DWC in a finite-difference time-domain (FDTD) simulation. Just to observe the spectral evolution from the DWC, we use a one-dimensional model without considering the detailed structure of the LSPCW. Here, a signal pulse with a full width at half-maximum (FWHM) of 0.8 ps and a center wavelength of 1550 nm is excited in a medium with $n = 3$ and a change in index $\Delta n = -0.005$. This simulates TPA-induced carriers. The change in the index moves in the same direction as the signal pulse. We consider the following cases: changing the index such that it overtakes and is overtaken by the signal pulse, changing the speed v_c of the change in index, changing the group velocity v_s of the signal pulse, and changing their relative launch times. Having the index profile overtake the signal pulse may appear superluminal, but it is possible by using slow-light pulses. The index decreases quickly and linearly, while remaining constant because the carrier lifetime is sufficiently long. If the control and signal pulses have the same FWHM, the FWHM of the TPA probability will be 0.56 ps because of the quadratic dependence of TPA on pulse intensity. Thus, we use it as the duration of index reduction. To simplify the analysis, loss and dispersion are neglected.

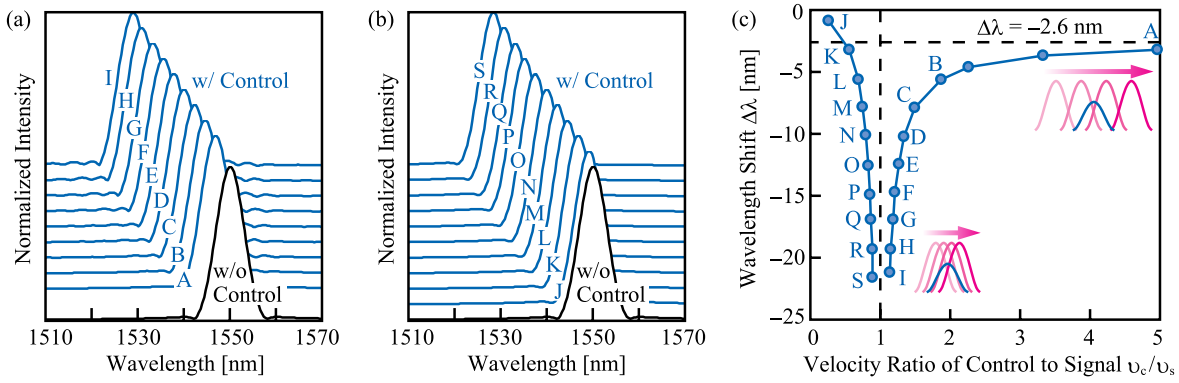

FIG. 3 (color online). FDTD simulation of DWC with 10 nm cell size and 20 as time step. Output signal spectra observed (a) when temporal change in index overtakes the signal pulse (curves $A-I$ correspond to $L = 70-460$ μm) and (b) when temporal change in index is overtaken by the signal pulse (curves J–S correspond to $L = 20-470$ μm). (c) Wavelength shift $\Delta\lambda$ evaluated from weighted center of spectra for v_c/v_s. Points $A-I$ and J–S correspond to the curves in (a) and (b), respectively. Inset show schematically the velocity difference between the signal pulse (depicted as stopped) and control pulse that produces the shift in index (depicted as moving).

Figures 3(a) and 3(b) show the simulated signal spectra for the cases in which the change in index overtakes and is overtaken, respectively, by the control pulse. In both cases, the signal pulse is blueshifted by the decrease in the index and the longer interaction length enhances this shift. Because the index change is linear, the spectral shape is well maintained, which is a feature of DWC. Figure 3(c) shows $\Delta\lambda$ calculated as a function of the velocity ratio v_c/v_s. When v_c/v_s approaches unity, $|\Delta\lambda|$ increases drastically because the index change overlaps the signal pulse entirely so that the signal spectrum is continuously converted (this increase spectrum is actually restricted by losses in the control pulse). When v_c approaches zero, $\Delta\lambda$ approaches zero. At $v_c = 0$, the signal pulse simply enters the region when the index is n (and leaves the region where the index is $n - \Delta n$). Thus, DWC does not occur. When $v_c \gg v_s$, the signal pulse seems to almost stop with respect to the control pulse and $\Delta\lambda$ converges to -2.6 nm, which satisfies $\Delta\lambda/\lambda \approx \Delta n/n$ for conventional DWC. Thus, Fig. 3 exactly shows the transition between conventional DWC and TD-DWC.

Next, we demonstrate TD-DWC experimentally. We launch a signal pulse and a more intense control pulse into a Si LSPCW fabricated by a CMOS-compatible process [12] and observe DWC in the signal pulse by using an optical spectrum analyzer. Details of the optical setup and the characteristics of the LSPCW are given in Ref. [11]. The LSPCW has a low-dispersion photonic band and a slightly dispersive band on the short-wavelength side. We can change the group velocity of the signal pulse by changing the input wavelength within the dispersive band. In the FDTD simulation, we changed the speed at which the index changes. However, in the experiment, changing the group velocity of the control pulse also changes the internal peak intensity because of spatial compression, resulting in different TPA rates. To avoid this, we changed the group

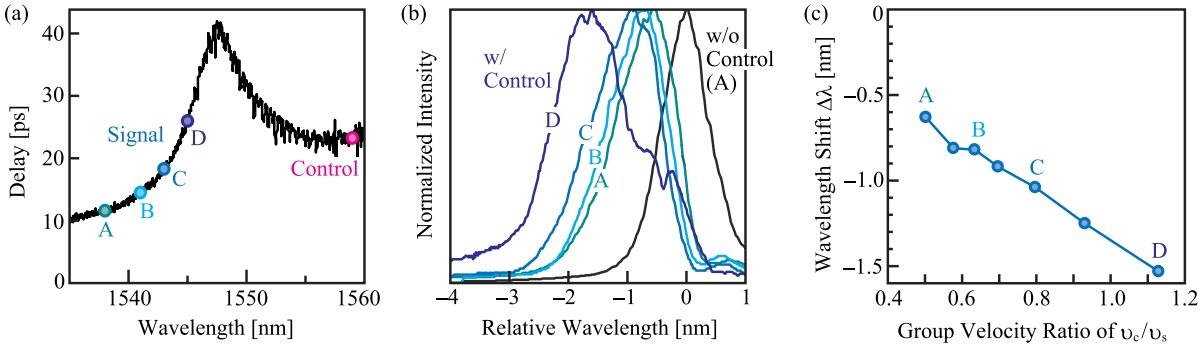

FIG. 4 (color online). Experimental results of TD-DWC. (a) Group-delay spectrum of air-cladded LSPCW and input wavelengths of signal pulse (1.9–2.7 ps in width and 1.2–2.7 W in peak intensity) and control pulse (5.6 ps, 22 W). In the LSPCW, the slab thickness is 210 nm, lattice constant is 450 nm, air-hole diameter is 240 nm, lattice shift is 120 nm, and waveguide length is 200 μm. (b) Output signal spectra. Conversion efficiencies evaluated from the integral of the spectrum are 45%–62%. (c) Wavelength shift for group-velocity ratio of two pulses.

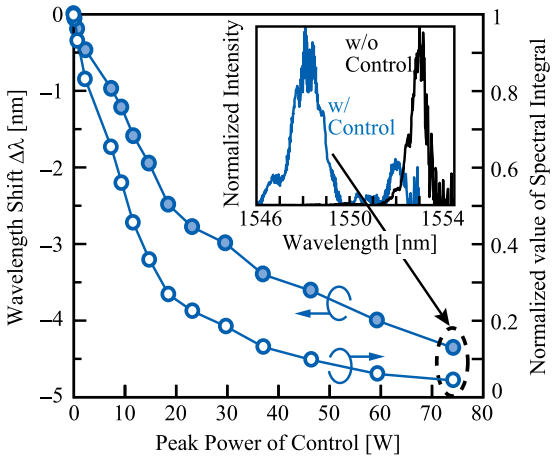

FIG. 5 (color online). Wavelength shift $\Delta\lambda$ and conversion efficiency measured as a function of peak power of control pulse evaluated from weighted center and integral of each spectrum, respectively. Inset shows spectra with and without control pulse.

velocity of the signal pulse. Figure 4(a) shows the measured group-delay spectrum of the LSPCW. By changing the input wavelength of the signal pulse from point A to D, its group delay increases (group velocity decreases). Since the wavelength of the control pulse is set at 1558 nm (red circles), the interaction length is maximized when the signal wavelength is set around the point D.

Output spectra are shown in Fig. 4(b). When the control pulse is present, the signal pulse is increasingly blueshifted in going from point A to D. The shape of the shifted spectrum is relatively constant from point A to point C but slightly broadens at point D. The carrier generation rate and spectral shift differ depending on whether the signal pulse overlaps with the peak or the feet of the control pulse. When the interaction is long (case D), this variation reflects the spectral broadening. If a rectangular control pulse is available, the signal-pulse shape is still maintained. Figure 4(c) summarizes the wavelength shift as a function of the group velocity ratio. The shift increases as the ratio increases. When the ratio is slightly greater than unity (case D), the shift continues to increase. Under these conditions, the group velocity increases after the blueshift near the input end of the waveguide because of the group-velocity dispersion shown in Fig. 4(a). This reduces the ratio towards unity; for this reason, the result of case D is different from the calculation in Fig. 3(c), which neglects dispersion.

Figure 5 shows the maximum blueshift observed by optimizing the signal wavelength and increasing the peak power of the control pulse. Upon increasing the power, the wavelength shift is saturated and the conversion efficiency is reduced because both pulses are attenuated, mainly by free-carrier absorption. At 74 W, the blueshift evaluated from the spectral peak reaches 4.9 nm. This is a very large DWC, which indicates the advantage of our approach.

Finally, we comment on the relationship between DWC and the Doppler effect. The comparison is valuable because both generate adiabatic spectral shifts, and the Doppler effect has been suggested to occur in photonic crystals [16]. For a wave source and observer moving with velocities v_1 and v_2, respectively, the common Doppler effect shifts the original wave frequency f to an observed frequency $f' = f(v_0 - v_2)/(v_0 - v_1)$ for constant phase velocity v_0. Here, the origins of $\Delta f = f' - f$ are the wave-number shift Δk and the direct shift of the observed frequency (see Table I). In addition, the Doppler effect also occurs for light reflected by a mirror moving with velocity u. Here, the origin is Δk at the reflection and $f' = f(v_0 - v_2)(v_0 + u)/(v_0 - v_1)(v_0 - u)$ for all effects. However, for DWC, the origin is the change in phase velocity Δv_0 during propagation. Even for conventional resonator-based DWC, the temporal change in index gives the effective Δv_0 with constant k. In our approach, the motion of the temporal change in index gives both Δv_0 and Δk. These DWCs appear similar to the mirror-type Doppler effect in the sense that the origins of Δf are in the optical path. However, they should still be regarded as different phenomena because of their different origins.

In conclusion, DWC is a unique phenomenon that achieves a pure spectral shift in a compact device with moderate power consumption. TD-DWC, demonstrated here, is a more generalized phenomenon that includes conventional resonator-based DWC and physically links conventional DWC and XPM. However, the origin of its frequency shift differentiates it from the Doppler effect. DWC can be generated by any type of temporal change in index in the presence of signal light and can be enhanced by a long interaction length. Slow light is a powerful tool that can control both of these parameters. We demonstrate

TABLE I. DWC compared with Doppler effects. Positions of wave source and observer are given by z_1 and z_2, respectively. Motion of observer causes Δf, without any changes of light.

Phenomenon	Type	Arising position	Origin of f'	InvariantFactor
DWC	Conventional approach	Optical path	Δv_0	z_1, z_2, k
	This approach	Optical path	Δv_0, Δk	z_1, z_2
Doppler effects	Motion of source	Light source	Δk	v_0
	Motion of observer	Observer	Δf	v_0, k
	Motion of mirror	Optical path	Δk	z_1, z_2, v_0

TD-DWC by using two copropagating slow-light pulses in a Si LSPCW and obtain an extremely wide spectral shift (up to 4.9 nm). Using free carriers causes loss, but the conversion efficiency is still better than that of parametric processes, which makes practical applications of this method look promising.

This work was partly supported by the FIRST Program of JSPS and the Future Pioneering Projects of NEDO.

[1] M. F. Yanik, and S. Fan, Phys. Rev. Lett. **92**, 083901 (2004).
[2] M. Notomi, and S. Mitsugi, Phys. Rev. A **73**, 051803 (2006).
[3] Y. Tanaka, J. Upham, T. Nagashima, T. Sugiya, T. Asano, and S. Noda, Nat. Mater. **6**, 862 (2007).
[4] S. F. Preble, Q. Xu, and M. Lipson, Nat. Photonics **1**, 293 (2007).
[5] J. Upham, Y. Tanaka, T. Asano, and S. Noda, Appl. Phys. Express **3**, 062001 (2010).
[6] Y. Xaio, G. P. Agrawal, and D. N. Maywar, Opt. Lett. **36**, 505 (2011).
[7] D. M. Beggs, T. F. Krauss, L. Kuipers, and T. Kampfrath, Phys. Rev. Lett. **108**, 033902 (2012).
[8] G. P. Agrawal, *Nonlinear Fiber Optics* (Academic, Boston, 2007), 4th ed.
[9] D. A. Farias, and J. N. Eckstein, IEEE J. Quantum Electron. **39**, 358 (2003).
[10] M. Notomi, H. Taniyama, S. Mitsugi, and E. Kuramochi, Phys. Rev. Lett. **97**, 023903 (2006).
[11] K. Kondo, M. Shinkawa, Y. Hamachi, Y. Saito, Y. Arita, and T. Baba, Phys. Rev. Lett. **110**, 053902 (2013).
[12] M. Shinkawa, N. Ishikura, Y. Hama, K. Suzuki, and T. Baba, Opt. Express **19**, 22 208 (2011).
[13] C. Monat, B. Corcoran, M. Ebnali-Heidari, C. Grillet, B. J. Eggleton, T. P. White, L. O'Faolain, and T. F. Krauss, Opt. Express **17**, 2944 (2009).
[14] M. F. Saleh, W. Chang, P. Hölzer, A. Nazarkin, J. C. Travers, N. Y. Joly, P. St. J. Russell, and F. Biancalana, Phys. Rev. Lett. **107**, 203902 (2011).
[15] Q. Lin, O. J. Painter, and G. P. Agrawal, Opt. Express **15**, 16 604 (2007).
[16] E. J. Reed, M. Soljačić, and J. D. Joannopoulos, Phys. Rev. Lett. **90**, 203904 (2003).